Cu_2O/CuO heterojunction catalysts through atmospheric pressure plasma induced defect passivation

Avishek Dey[a], Gauthaman Chandrabose[a], Lois A.O Damptey[a], E. S. Erakulan[b], Ranjit Thapa[b], Siarhei Zhuk[c], Goutam Kumar Dalapati[a,b,c*], Seeram Ramakrishna[d], Nicholas St. J. Braithwaite[a], Amir Shirzadi[a], and Satheesh Krishnamurthy[a*]

[a]School of Engineering and Innovation, The Open University, Milton Keynes, MK76AA, UK

[b]Department of Physics, SRM University – AP, Amaravati 522502, Andhra Pradesh, India

[c]Institute of Materials Research and Engineering, A*STAR (Agency for Science, Technology and Research), 2 Fusionopolis Way; Innovis, #08-03, Singapore 138634

[d]Center for Nanofibers and Nanotechnology, National University of Singapore, Singapore-117576

E-mail address: satheesh.krishnamurthy@open.ac.uk (S. Krishnamurthy),

goutam.d@srmap.edu.in (G K Dalapati)

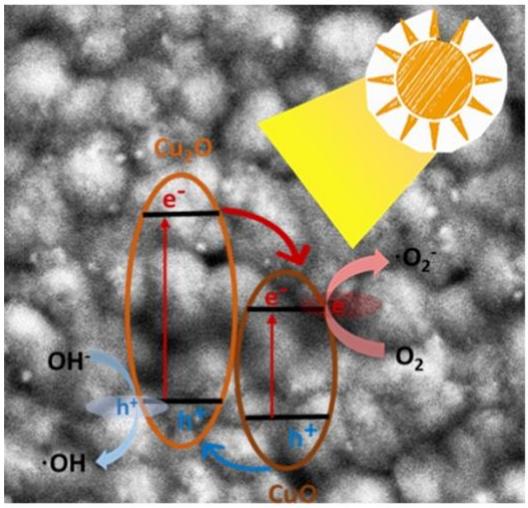

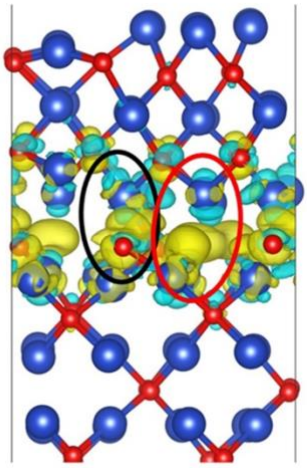

Epitaxial growth of CuO nanostructures on Cu_2O films using atmospheric pressure plasma jet is demonstrated, that can operate without the need of transparent current collector.

Highlights

- Fast and environment friendly route for CuO/Cu_2O heterojunction synthesis.
- Epitaxial growth using atmospheric pressure plasma jet.
- The heterojunction electrodes can operate without transparent current collector.
- High currents and stability towards electrocatalysis and photocatalysis.

Abstract

A novel route to fabricate Cu_2O/CuO heterojunction electrodes using an atmospheric pressure plasma jet (APPJ) is demonstrated. This process promotes favourable band alignment and produces nanoscale CuO surface features from Cu_2O with low density of interfacial defects. This electrode can operate without any transparent current collector, showing remarkable currents and stability towards oxygen evolution reaction (OER) (6 $mAcm^{-2}$ for 2 hours at pH14) as well as photocatalytic hydrogen evolution reaction (HER) activity (-1.9 $mAcm^{-2}$ for 800 seconds at pH7). When the electrocatalytic oxygen evolution (OER) activity was measured for Cu_2O/CuO electrode deposited on FTO substrate the currents increased to ~ 40 $mAcm^{-2}$ at 0.8V vs SCE in 1 M KOH without compensating for the electrode electrolyte surface resistance (*iR* correction). The composite films also exhibited a high rate towards photo degradation of Methylene Blue (MB) and phenol in the visible spectra, indicating efficient charge separation. We modelled the electronic structure of this epitaxially grown Cu_2O/CuO heterojunction using density functional theory. The calculations revealed the distinctive shifts towards Fermi level of the *p*-band centre of O atom in Cu_2O and *d*-band centre of Cu atom in CuO. at the interface contribute towards the increased catalytic activity of the heterostructure. Another factor influencing the activity stems from the high density of excited species in the plasma introducing polar radicals at the electrode surface increasing the electrolyte coverage. This work presents the potential of APPJ functionalization to tune the surface electronic properties of copper oxide based catalysts for enhanced efficiency in OER and HER water splitting.

Keywords: Heterojunction, Cu_2O, CuO, OER, HER, Photocatalysis.

1. Introduction

Harvesting energy from renewable sources is key, to fight with global warming towards the development of carbon free environment. Producing fuels using solar energy is one of the sustainable solutions to overcome the current global challenges of energy and environment. [1] Due to the abundance of sunlight, photo-electrochemical splitting of water into hydrogen and oxygen is the most promising approach to generate clean energy. [2] Electrochemical or photo-electrochemical water splitting involves two half-cell reactions: hydrogen evolution reaction (HER) at the cathode and oxygen evolution reaction (OER) at the anode.[3] The kinetics of this reactions are vastly different. OER is a four electron-proton coupled reaction ($2O^{2-} \rightarrow O_2 + 4e^-$) while HER is only a two electron-transfer reaction ($2H^+ + 2e^- \rightarrow O_2$) . [4] Hence OER is kinetically more sluggish and requires higher energy than the theoretical potential of 1.23 V.[5] Over the years noble metals such as Pt , Ru , Ir and composites have been considered as the state-of-the-art electro-catalysts for OER and HER. But the scarcity and high cost are the major drawbacks for their use in large scale applications. RuO_2 and IrO_2 show the highest performance and are typically used as benchmark for OER, Pt is used as the standard for HER.[6,7] Still, these metal oxides require over-potentials of hundreds of millivolts in order to achieve 10 mA/cm^2 of OER current. They also get oxidised to form RuO_4 , IrO_3 and get dissolved in the electrolyte during OER process. [4] Additionally the high cost and low abundance of these materials restrict their large-scale implementation. Hence, to make the process of water splitting cost effective it is desired to develop catalysts from nontoxic, low cost and earth abundant elements.

In recent years, first row transition metal-based oxides have attracted considerable attention for electrochemical water splitting applications.[4,8,9] Copper is naturally abundant, inexpensive and possess rich redox properties, thus offers the potential for large-scale application in catalysis. Several Cu based nanostructured oxides and model complexes have

been reported as catalysts ,including electro-catalysts and photo-catalysts . [10–14] Both CuO and Cu_2O are inherently *p*-type and have shown promise as photocathodes for water splitting due to their suitable position of conduction band edges with respect to the potential for H_2O/H_2. [15–18]. Recently, the oxides of Cu have been investigated for electro-catalytic OER and intense research is still being pursued to address the challenge of high onset over-potential. [8,19]

Cu_2O in one of the ideal candidates for solar driven photo-catalysis due to it direct band gap of 2 eV and theoretical solar to fuel conversion efficiency of 18% and photocurrent density of 14.7 $mAcm^{-2}$.[20] On the other hand, CuO ,with a band gap of ~1.5 eV is ideal candidate to absorb larger portion of the solar spectrum and is capable of producing a theoretical maximum photocurrent of 35 $mAcm^{-2}$ under standard AM1.5 irradiation.[16] Moreover, the position of its conduction band edge at -3.66 eV with respect to vacuum is suitably placed to evolve hydrogen from water. Though Cu_2O and CuO both have demonstrated potential for photocatalytic water splitting (oxidation/reduction) but their high recombination rate and susceptibility towards photo-corrosion prevent these two materials from being highly efficient photocathodes.[21] There have been several reported strategies to overcome the above problems associated with Cu_2O and CuO. One of them is to load co-catalysts like Pt, RuOx , Au-Pd and MoS_{2+x}. [22–25] Another method is to construct heterojunctions with *n*-type semiconductors with more positive conduction band position like ZnO, TiO_2 to promote the efficient separation of photo-generated charge carriers.[20,26–30]. Coating with graphene and carbon has also proved to be effective to combat the photo-corrosion stability. [31,32] Recently Wu et al. ha reported that by introducing a ultrathin amorphous layer of ZnO between Cu_2O/TiO_2 heterojunction on FTO, the stability of Cu_2O electrode can be increased for photoelectrochemical water splitting. [33]

One of the most interesting and challenging methodology is to create a Cu_2O/CuO heterojunction, to harness the properties of both these *p*-type copper oxides. It has been reported that by using a CuO over layer can enhance the stability of Cu_2O and provide a suitable band structure for charge transportation. [18,21,34–37] This is because the conduction and valence band edges of Cu_2O are at more negative potentials with respect to CuO. Hence, the photogenerated electrons in the conduction band of Cu_2O will be injected into that of CuO, whereas the photogenerated holes in the valence band of CuO are injected into that of Cu_2O at the Cu_2O/CuO interface.[21] Additionally, the formation of CuO overlayer on the Cu_2O can enhance the activity towards OER. It has been proven that CuO is catalytically more active while Cu_2O is more robust towards OER. Oxygen evolution at the CuO surface is preceded by the transformation of Cu^{2+} to Cu^{3+} species. Being unstable, these Cu^{3+} species dissociate to $Cu^{2+}O$ and O_2.[38] This repeated cycling of Cu^{2+}oxide−Cu^{3+}oxide drives the OER activity at the CuO anodes. However, this process also leads to the dissolution of the catalyst and eventually cessation of its activity. Thus, having a Cu_2O support is key to the charge kinetics at the electrode electrolyte interface. Cu_2O when kept at sufficient anodic potentials for longer durations, slowly converts to CuO.[17] Thus, replenishing the top CuO surface and enhancing the stability of the electrode. To prove this hypothesis, Cu_2O/CuO composite electrodes were fabricated on bare glass substrates without any current collector and were tested for OER activity.

However, the fabrication of Cu_2O/CuO heterojunction electrodes faces many challenges such as (a) good interfacial charge transfer properties through favourable band alignment is hard to achieve, (b) lattice distortion at interface creating high density of defect states at the interface. These defects act as trapping sites for charge carriers, leading to degraded photocurrent and photovoltage values. [39] Till date Cu_2O/CuO heterojunction has been synthesized using several methods such as sputtering [40], chemical vapor deposition [41], annealing [18], electrodeposition [21,39] and

sol–gel approaches. [35] But all these techniques either need sophisticated vacuum equipment's or complex chemistry. Here in we demonstrate an environment friendly route for the synthesis of Cu_2O/CuO heterojunction using atmospheric pressure plasma jet (APPJ) functionalisation techniques. An APPJ produces high flux of neutral, charged and ionized species and can simultaneously control the microstructure, morphology, and electronic structure of the exposed material. Because of the low penetration depth, the changes happen at the very surface of the material being treated, Cu_2O in this case. Our previous studies using X-ray absorption spectroscopy in total electron yield and total fluorescence yield revealed that the plasma jet induced chemical changes can occur up to 50-100 nm at the surface.[42] Cu_2O is known to be the least stable during electrochemical and photochemical processes. Cu_2O is prone photo corrosion. A possible way to enhance its stability is to add a thin layer of CuO on top creating a favourable band alignment. Here the CuO top layer grows from the Cu_2O base, hence a diffused junction is formed at the interface reducing the defect sites. With plasma functionalization the catalytic performance and stability of the Cu_2O photocathode enhanced significantly towards OER and HER. An OER current or 6 $mAcm^{-2}$ at pH14 and HER current of 1.9 $mAcm^{-2}$ at pH7 was obtained. Which is significantly high considering no current collector was involved when compared previous reports. Note, the photocurrent achieved here is more than twise the values reported Wu *et al*. for a TiO_2/ZnO/Cu_2O heterojunction device prepared via pulsed electrodeposition technique.[33] Also, the Cu_2O/CuO composite electrode showed an impressive OER stability for 2 hours. In addition, we also investigated the degradation of Methylene Blue dye using these films and found the functionalized films show higher degradation rate. This work with APPJ is an exciting new route to surface engineer highly efficient Cu_2O/CuO bilayer composite catalyst for water splitting.

2. Experimental details

2.1 Electrode preparation

CuO thin films were first deposited onto FTO coated glass and quartz substrates using magnetron sputtering. Substrates were first ultrasonicated in IPA for 10 mins and dried in a nitrogen gas flow. After cleaning, the substrates were loaded into the sputtering chamber for CuO thin film deposition. The deposition was carried out at room temperature using stoichiometric CuO target and argon ambient. The chamber was first pumped down to achieve a high vacuum of 6×10^{-4} mTorr and was then operated at 3 mTorr working pressure. The sputtering rate was optimized to achieve CuO films with average thickness 300 ± 30 nm. After deposition, the CuO films were then subjected to thermal annealing (Jet First 150, Jipelec) in nitrogen ambient at 550 °C for 30 min with the heating and cooling rate of 15 °C s^{-1} respectively to achieve Cu_2O films.

To create heterostructure, the Cu_2O films were annealed at 350 °C and simultaneously exposed to an atmospheric pressure plasma jet (APPJ) for 5 minutes to surface functionalize these annealed films. The films were kept at a minimum optimised distance of 5 mm to avoid any arcing between the sample and electrodes [43]. In this case the plasma jet was operated at a frequency of 13.56 MHz and 12 dBm rf level. With helium flow rate of 2 standard liters per minute (slm) and oxygen (2% of helium) the measured power dissipated was 5 watts. Scheme 1 illustrates the flowchart for the synthesis of Cu_2O/ CuO heterojunction electrode.

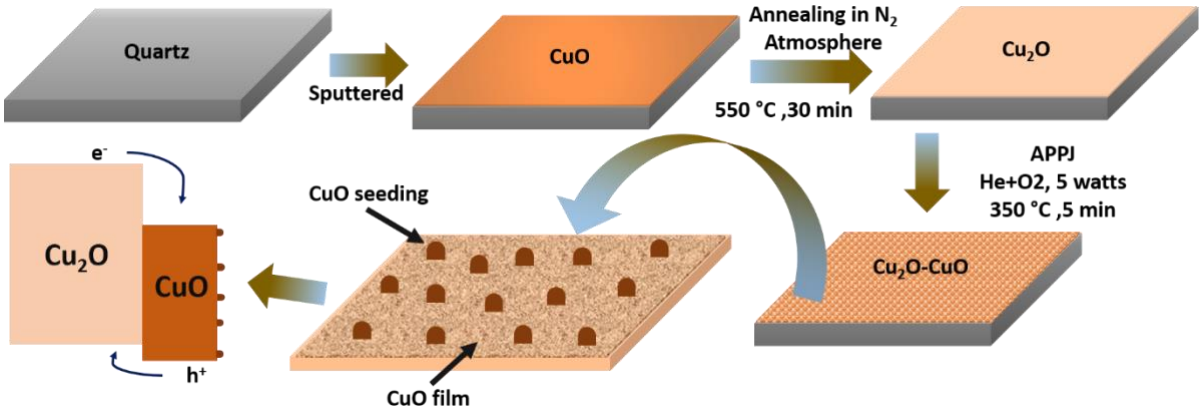

Scheme 1. Flowchart of the synthesis process for Cu_2O/CuO heterojunction electrode

2.2 Electrochemical and Photoelectrochemical measurements

Electrochemical measurements were carried out using Autolab PGSTAT M204 potentiostat/galvanostat equipped with a FRA32M module using a three-electrode configuration consisting of Pt counter electrode, saturated calomel reference electrode (SCE), and the thin films as working electrode. Copper wires were attached to the substrates using silver paste. For some substrates, current was collected from FTO and for others without FTO the top of the Cu_2O films acted as electrical contact. The substrates were then covered on the sides with polypropylene tapes to prevent any electrolyte leakage, leaving a square active area on the substrate. 1 M KOH (pH 13.8) and pH7 buffer electrolyte (HI-7007L, Hanna instruments) were used as electrolytes for these measurements. Asahi spectra HAL-320 with solar simulator was used as the light source equipped with an air mass 1.5 global (AM 1.5G) filter and a 300 W xenon arc lamp, was used as the illumination source. The light intensity on the CuO electrode was measured using a Si photodiode and maintained at 1 sun illumination. Linear sweep voltammetry (LSV) were measured at a scan rate of 5 mV s^{-1} while

chronoamperometry (CA) were obtained at a potential of 0.35 V vs. RHE. Electrochemical impedance spectroscopy (EIS) was performed at an applied potential of 0.35 V vs RHE and 10 mV amplitude over the frequency range of 0.1 Hz to 100 kHz.

The photocatalytic activity of CuO (Annealed and Plasma Treated) thin-film samples were also evaluated by monitoring the degradation of organic pollutants, irradiated under xenon light source. Thin-film sample (10mm x 10mm) was placed inside the glass vessel containing 20 mL of MB and phenol solution (10mg/L in deionized water) and the light source (300 W, 75mW/cm^2, 350-1100nm, AM1.5G filter) is illuminated from the top with a distance of 20cm from the liquid surface. The intensity of the light source was tuned to attain 1 SUN condition and the light illuminated area was maintained about 30mm x 30mm. Under the dark condition, the solution was magnetically stirred (150 RPM) for 30 minutes at room temperature to attain the adsorption/desorption equilibrium. During the 3 hours of light illumination, 1 mL aliquot of the MB solution were collected at a time interval of every 30 mins. The liquid samples are transferred into a quartz cuvette (M/s. Hellma) and absorption spectra were recorded by using UV-vis spectrophotometer (M/s. Thermo Scientific, Evolution 220).

2.3 Material characterization

Surface morphology of the samples was investigated scanning electron microscope (SEM), Zeiss Supra 55VP. Raman spectra were measured using a Horiba Jobin-Yvon LabRAM HR evolution spectrometer and an argon ion laser (514.5 nm) was used as the excitation source. To understand the surface chemical and electronic properties of these thin films X-ray photoelectron spectroscopy spectra (XPS) were recorded on a load-locked Kratos XSAM800. Mg Kα (1253.6 eV) operated at 12 kV and 10 mA was the excitation source. Throughout the measurements base pressure of the chamber was maintained below 10^{-9} mbar. High magnification analyzer mode was chosen to collect electrons from an area of 4.0 mm^2 on the

specimen. Binding energy values were calibrated to C1*s* peak of adventitious carbon (285 eV). All core lines were analyzed using a Shirley background subtraction algorithm and fitted with a mixture of Gaussian for instrumental effects and Lorentzian line shape function for core hole effects (50% weightage each) to keep the residue (χ^2) <1. To map the changes surface potential with plasma functionalization Kelvin probe force microscopy (KPFM) was performed on these films using an Asylum Research MFP-3D with Pt−Ir-coated conducing silicon probes (PPP-EFM, Nanosensors) with a nominal force constant of 2.8 N/m used for this measurement. The tip was biased at +3 V for the KPFM scan with a drive amplitude of 300 mV. The surface potential was mapped on an area of 1 μm^2 with scan rate of 0.5 Hz and 512 points and lines.

2.4 Computational details:

All the calculations are performed using spin polarized density functional theory as implemented in the Vienna Ab-initio Simulation Package (VASP). [44] Projected Augmented Wave (PAW) method is used to describe the potentials of the atoms. [45] Generalized Gradient Approximation (GGA) is considered for exchange and correlation effects at Per dew-Burke-Ernzerhof (PBE) level. [46] Plane wave cut-off energy of 400 eV is used for the calculations. Monkhorst Pack scheme with a 2x2x1 K-point grid is used for the Brillouin zone sampling. Structural optimizations were done until the total energy converged less than 10^{-4} eV per atom and the maximum force converged less than 10^{-3} eV/Å. As a model structure we have made heterostructure of CuO/Cu_2O along 001 directions. 2x2x1 supercell is taken for CuO-001 surface and 2x2x2 supercell is consider for Cu_2O surface to build the heterostructure. Vacuum of ~10 Å along the z-direction is taken to avoid the spurious interaction. The CuO has Cu atoms at the interface and Cu_2O has oxygen atoms at the interface.

3. Results and discussion

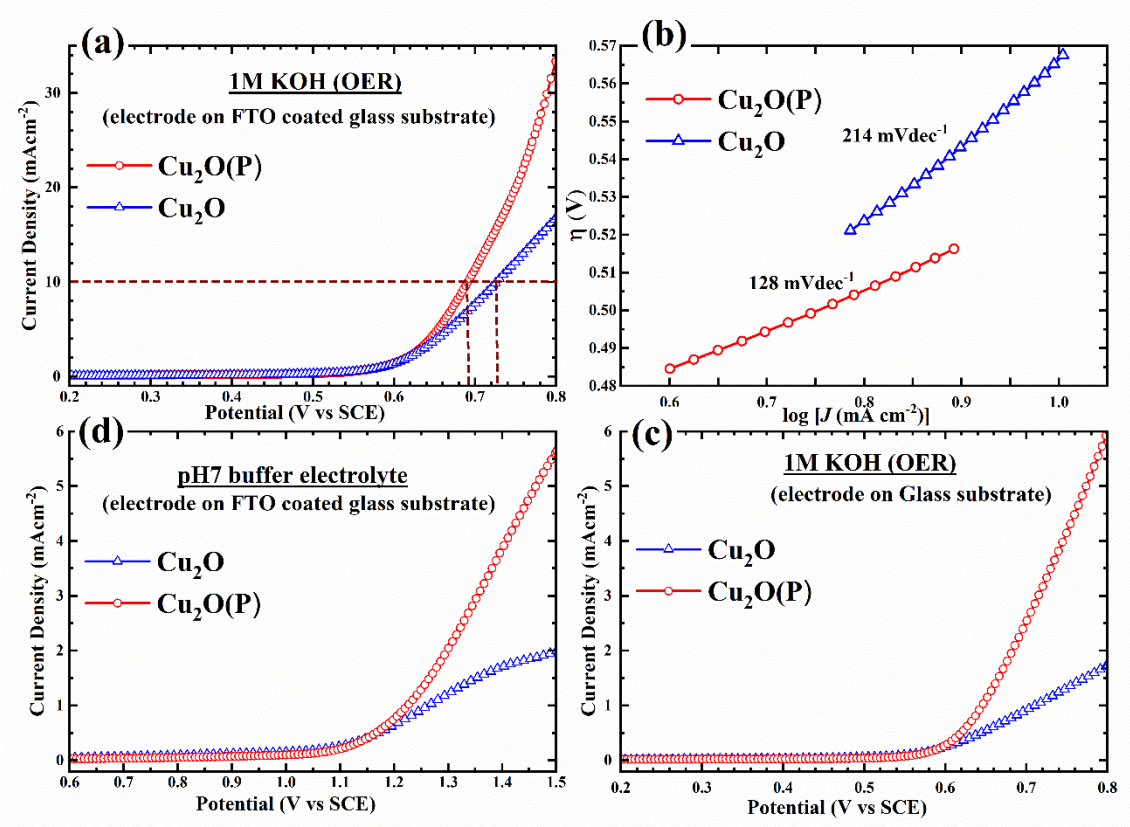

Fig. 1. (a) Electrochemical OER performance of Cu_2O and Cu_2O/CuO in 1M KOH, (b) corresponding Tafel curves, (c) electrochemical OER performance of Cu_2O and Cu_2O/CuO in pH7 buffer electrolyte, (d) electrochemical OER performance of Cu_2O and Cu_2O/CuO in 1M KOH (without current collector). All LSV curves are non-*iR* compensated and at scan rate: $5mvs^{-1}$.

The impact of plasma functionalisation on the catalytic properties of the Cu_2O films were investigated through electrochemical oxygen evolution (OER) and photoelectrochemical hydrogen evolution reaction (HER). Linear sweep voltammetry (LSV) was used to test the samples both for electrocatalytic and photocatalytic properties in a three-electrode configuration, Pt wire as the counter electrode and SCE (4M KCL) as the reference electrode.

It is to be noted that all the plots have not been compensated for the iR drop, which appears at the solid electrolyte interface. From the LSV curves, current density of the electrode was determined. Fig. 1 shows the comparative OER activities of pristine and plasma functionalised Cu_2O films both in alkaline (pH 14) and neutral pH conditions (pH 7) taken at a scan rate of 5 mVs^{-1}. In 1M KOH (Fig. 1 (a)) the plasma functionalized thin films show a catalytic current density of 34 $mAcm^{-2}$, twice as much the pristine sample which could achieve 16 $mAcm^{-2}$ at 0.8 V vs SCE (1.8 V vs RHE). The onset potentials for these samples started at the same position but the composite films require a considerably lower overpotential of ~ 40 mV with respect to the pristine sample to achieve a current density of 10 $mAcm^{-2}$. Fig. 1 (b) shows the measured Tafel slope of the composite film is 128 mV dec^{-1} which is far smaller than the pristine Cu_2O film having a Tafel slope of 214 mV dec^{-1}. This suggests that, with plasma functionalisation the reaction kinetics towards OER has improved considerably. Similar increase in catalytic activity was also observed in pH7 buffer electrolyte as well (Fig. 1 (c)). At 1.5 V vs SCE the plasma functionalised films showed a catalytic current density of 5.5 $mAcm^{-2}$ almost three times as the pristine sample that could achieve 2 $mAcm^{-2}$. The purpose of high temperature annealing is to increase the conductivity in the bulk of these sputtered thin films. Using four probe technique the average resistivity values were obtained as 413 Ω□□ for the annealed sample, and after plasma functionalization this value increased to 1.48 kΩ□□ . Fig. 1 (d) shows the OER activity of the Cu_2O and plasma functionalised Cu_2O films on a bare glass substrate. It was observed that the sputtered CuO films showed negligible catalytic activity without the current collector in 1M KOH. After being annealed the catalytic activity of these films improved and can be attributed to the increase in bulk conductivity. For the composite film drastic increase in current density is observed from 1.8 $mAcm^{-2}$ to 6 $mAcm^{-2}$. This improved bulk conductivity is critical to enhancing the activity of a catalytic material. However, surface morphology also plays a pronounced role in causing difference in catalytic

activity. [3] Christina *et al.* reported that heat treatment increases the roughness factor of the electrocatalyst creating more active sites on the surface which in turn boosts the catalytic performance of Cu(0)-based catalyst towards CO_2 reduction by. [47] The same films showed 80% retention of catalytic activity up to 2 hrs at a high applied potential of 0.8V vs SCE (Fig. 2 (c)). To the best of our knowledge, this is the first time we are reporting OER stability up to 2 hours on copper oxide electrode without using any current collector e.g. FTO or Ni foam. The photocatalytic HER activity of these samples were also tested in a pH7 buffer electrolyte under dark and under light (1 sun) conditions as shown in Fig. 2(a). To make H_2 evolution as the dominant cathodic reaction, the electrolyte was purged with N_2 to remove dissolved O_2. With plasma functionalisation the photo current increased to 1.9 $mAcm^{-2}$ with respect to the pristine Cu_2O sample which shows a meagre photocurrent of 0.65 $mAcm^{-2}$. Interestingly the dark current for the Cu_2O(P) is almost equal to the photocurrent of Cu_2O. Additionally the plasma functionalised Cu_2O films showed stability up to 800 seconds at a constant potential of 0.35 V vs RHE, which is excellent considering the Cu_2O films were damaged almost instantly during this test (Fig. 2 (d)). These results suggest that plasma functionalisation on the films facilitates the necessary band alignment for both OER and HER activities. As the charge transport properties are improved the stability also improved inevitably. Electrochemical impedance spectroscopy (EIS) has also been employed to discern the kinetics of charge transfer at the electrode electrolyte interface. Fig. 2 (b) shows the Nyquist plots of the two electrodes at a potential of 0.35 V vs RHE in pH7 buffer electrolyte. The semicircle feature of Nyquist plot at high frequencies is attributed to the redox charge transfer process at the interface and the diameter of the semicircle is represents the charge transfer resistance (R_{ct}). EIS of these electrode as in Fig. 2(b) shows the R_{ct} of Cu_2O is 7.2 kΩ and after plasma functionalisation decreases significantly to 2.1 kΩ. This decrease in R_{ct} stems from the accelerated charge transfer kinetics at the copper oxide/electrolyte interface. Similar decrease in R_{ct} was also

observed by Yang *et al.* for a Cu_2O/CuO bilayer composite structure.[21] However their composite structure showed $R_{ct} > 8\ k\Omega$, much higher than our electrode.

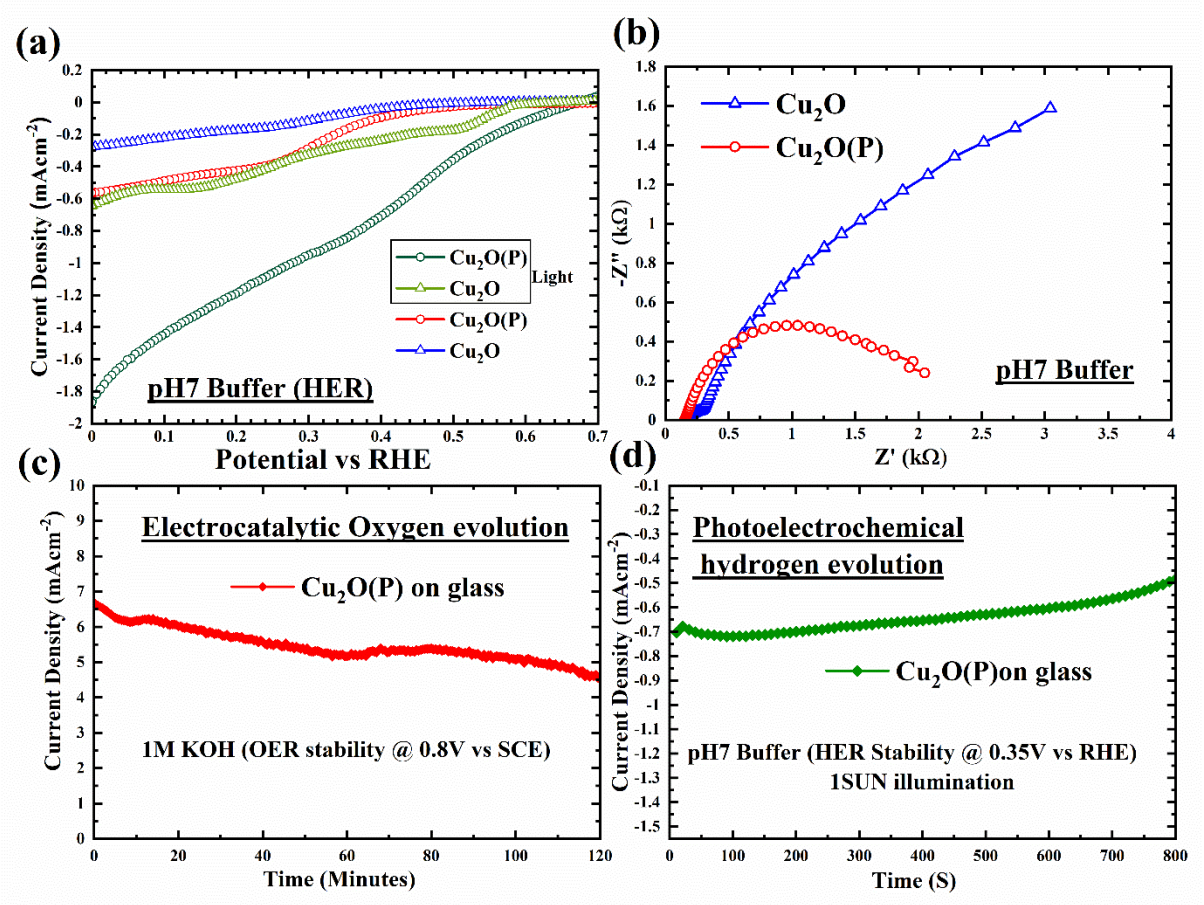

Fig. 2. (a) Photoelectrochemical response of Cu_2O and Cu_2O/CuO in pH7 buffer (b) EIS spectra of Cu_2O and Cu_2O/CuO in pH7 buffer, (c) OER stability of Cu_2O/CuO in 1M KOH (without current collector), (d) HER stability Cu_2O/CuO in pH7 buffer under 1 sum illumination (without current collector).

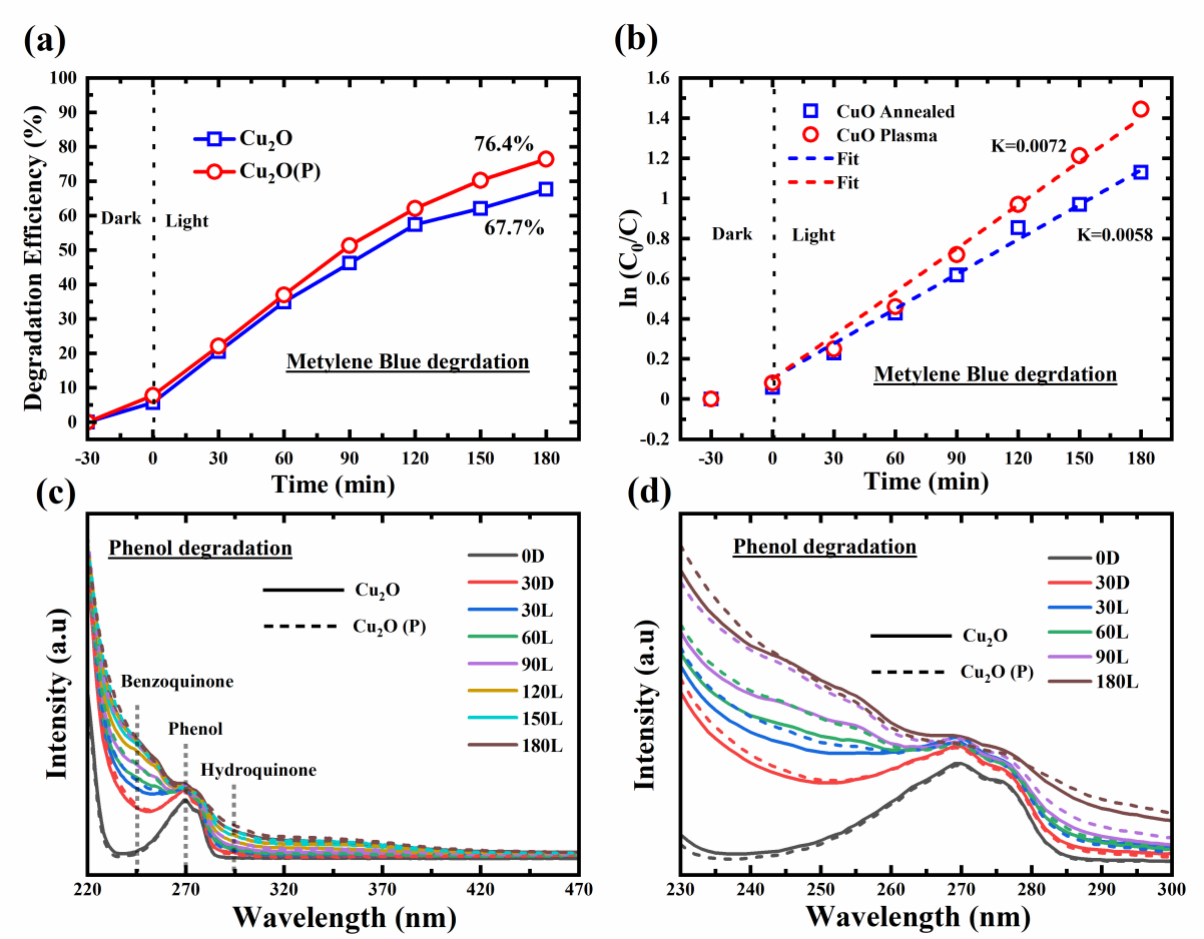

Fig. 3. (a) Photocatalytic degradation of methylene blue (b) corresponding degradation rate of MB for Cu_2O and Cu_2O plasma-treated (Cu_2O(P)) thin films under visible light irradiation, (c-d) UV-Vis absorption spectra for representing photocatalytic degradation of Phenol at different intervals of time. Samples kept in 30 minutes dark(D) to reach equilibrium before starting the photodegradation under simulated light (L).

The photocatalytic performance of CuO (Annealed and Plasma Treated) thin films under visible light condition are evaluated by analysing the photodegradation of MB for a periodic interval of time. MB (10mg/L) dye solution of 20mL volume was taken in a top-end opened glass made reactor vessel. The thin film sample (10mm x 10mm) was immersed in the dye solution and the solution medium is kept under constant magnetic stirring (RPM 150) throughout the experiment. In order to attain the adsorption equilibrium, the sample immersed

inside the dye solution was maintained under the dark condition for 30 minutes and after that, the Xenon light source optimized for 1 Sun condition was focused on the thin film sample by using collimator lens. During 3 hours of light illumination 1ml of the solution was collected for every 30 minutes and the liquid samples were characterized by UV-vis absorption spectroscopy to record the absorption peak of MB at 661nm. It has been reported that Cu_2O shows faster degradation rate for MB degradation under visible light degradation. [48] CuO annealed sample (i.e. Cu_2O) showed MB dye degradation efficiency about 67.69% with the degradation constant K of 0.0058 min^{-1} (Fig 3(b)). Whereas the plasma-treated sample with (i.e. Cu_2O/CuO) heterostructure showed better degradation efficiency (76.41%) and higher degradation constant (K = 0.0072 min^{-1}). This enhanced photocatalytic activity is attributed to the favourable band edge position of Cu_2O/CuO which exhibits a type II heterostructure (Fig. 5). Both oxides of copper have wide visible absorption spectra and when the light is irradiated on the sample, electrons are photoexcited to the conduction band leaving a valence hole behind. Due to the more negative energies of conduction band and valence band of CuO with respect to Cu_2O. The photoexcited electrons from Cu_2O gets transferred to the CB of CuO which further reacts with O_2 molecule to form an oxygen radical (superoxide, $\cdot O_2^-$). Whereas the holes from CuO gets transferred to the VB of Cu_2O and further reacts with hydroxide ion (OH^-) to generate hydroxyl radical (·OH) as shown in Figure 5. These radicals ($\cdot O_2^-$ and ·OH) undergoes multiple reactions with MB dye molecules and degrades the parent dye compound. Thus Cu_2O/CuO heterostructure sample reduces the charge recombination rate and enhance the photodegradation of organic dye molecules compared to Cu_2O sample. From the comparation presented in Table 1, it is evident that plasma functionalised Cu_2O could be a promising candidate for solar dye degradation application.

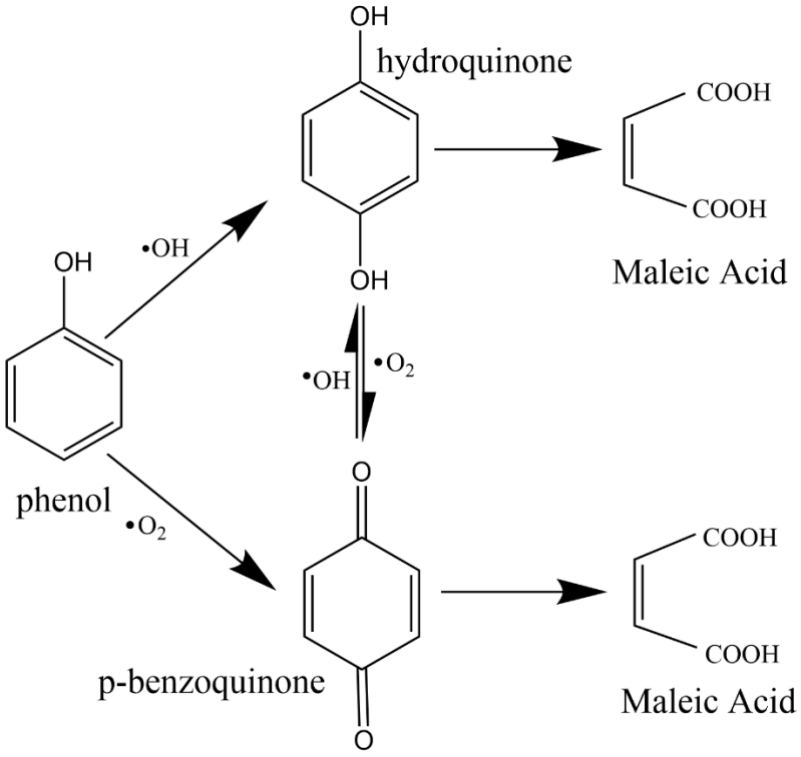

Fig. 4. Degradation pathways of phenol in the presence of photocatalyst and H_2O_2.

Phenol is one of the common organic pollutants found in industrial wastewaters, which includes chemical and petrochemical industries. [49] Adsorption using activated carbon is generally used to separate phenolic pollutants from aqueous media. Hence it is important to device alternate ways such as photo catalytic degradation to mineralize these pollutants. As a proof of concept, the enhanced photoactivity of the Cu_2O thin films after plasma functionalisation was studied using photodegradation of phenol. Here, the experiment parameters were kept same as in MB degradation with phenol concentration of 10mg/L. figure 3(c) and (d) shows the absorption spectra of the phenol suspension at regular intervals of time. For the pristine suspension the spectra only show the presence of phenol at 270 nm. With the addition of H_2O_2 and CuO photocatalysts the spectral feature changes due to the formation of benzoquinone and hydroquinone. It has been reported that the photo degradation of phenol occurs via the formation of p-benzoquinone and hydroquinone by the superoxide ($\bullet O_2^-$) and

hydroxyl radicals (•OH) respectively as shown in figure 4.[49] In the spectra presented here characteristic peaks of benzoquinone increase first followed by the rise in hydroquinone. Indicating that phenol is decaying through these two intermediate products firstly benzoquinone and then further decay via the formation of hydroquinone. The spontaneous production of $\bullet O_2^-$ from H_2O_2 decomposition led to the formation of benzoquinone even in the dark conditions. In the presence of light this reaction is accelerated by the photoinduced electron transfer to the catalyst surface causing faster decomposing of H_2O_2.[50] Moreover, H_2O_2 has been used here as the hole scavenger. The photo-generated holes react with H_2O_2 producing hydroxyl radicals as a strong oxidant that can breakdown phenol via multi step ring opening reaction. From figure 3(d) the plasma treated Cu_2O shows faster oxidative decay of phenol with respect to Cu_2O. The heterojunction catalyst is ahead by almost 30 mins in terms of phenol degradation as seen from the UV-Vis spectra. Notably, the changes in spectral features saturates after 90 mins for Cu_2O(P) while it takes 180 mins for pristine Cu_2O. The enhanced activity could be attributed to the higher concentration of photogenerated charge carriers in the Type II heterostructure of Cu_2O(P) emanating from ideal band alignment and lower recombination losses.

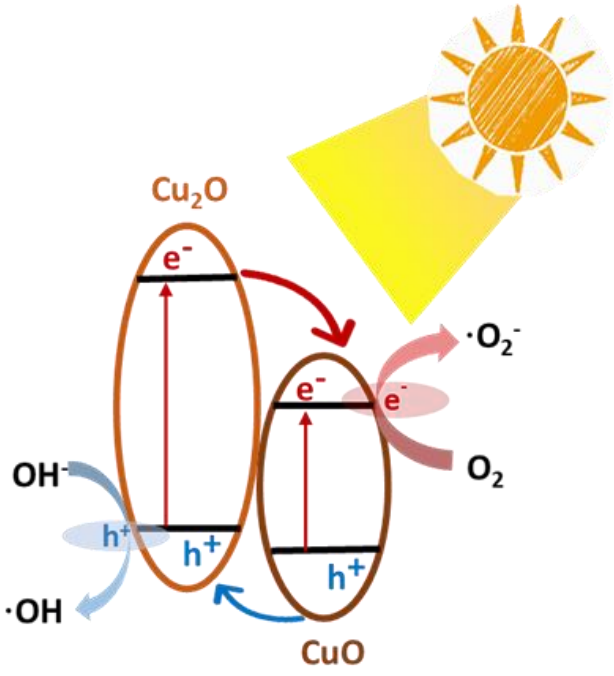

Fig. 5. Schematics of charge transfer promoting photocatalytic activity.

Thin film sample	**Method of synthesis / sample surface area**	**Dye molecule concentration / solution volume**	**Light Source / Degradation time / Degradation Rate/ Degradation efficiency**	**reference**
CuO	RF sputtering, 937.5 mm^2	MB (10 mg/L), 70 mL	Halogen lamp (150W), 3h, 74.3%	1
Cu_2O	RF sputtering, 937.5 mm^2	MB (10 mg/L), 70 mL	Solar Spectrum (100mW/cm^2), 3h, 98.8%	1
CuO	RF Sputtering (50W, 300°C), 150 mm^2	MB (10 mg/L), 20 mL	Xenon arc lamp (AM1.5G, 150W), 5h, K= 0.013 min^{-1}, 90%	2
CuO, Cu_2O, CuO-Cu_2O	RF Sputtering (200W), 150 mm^2	MB (10 mg/L), 20 mL	Xenon arc lamp (AM1.5G, 150W), 5h, CuO K= 0.013 min^{-1} / 78%, Cu_2O K=0.013min^{-1} / 80%, CuO–Cu_2O K= 0.021 min^{-1} / 90%	3
Cu_2O	Sputtering of CuO, 100 mm^2	MB (10 mg/L), 20 mL	Solar Spectrum (300W, 75mW/cm^2), 3h, K= 0.0058 min^{-1} 67.69%,	CW
CuO-Cu_2O	Sputtering of CuO, 100 mm^2	MB (10 mg/L), 20 mL	Solar Spectrum (300W, 75mW/cm^2), 3h, K= 0.0072 min^{-1} 76.41%,	CW

Table 1. The comparison of photocatalytic activity of copper oxide thin films for photodegradation of dye molecules with respect to current work.

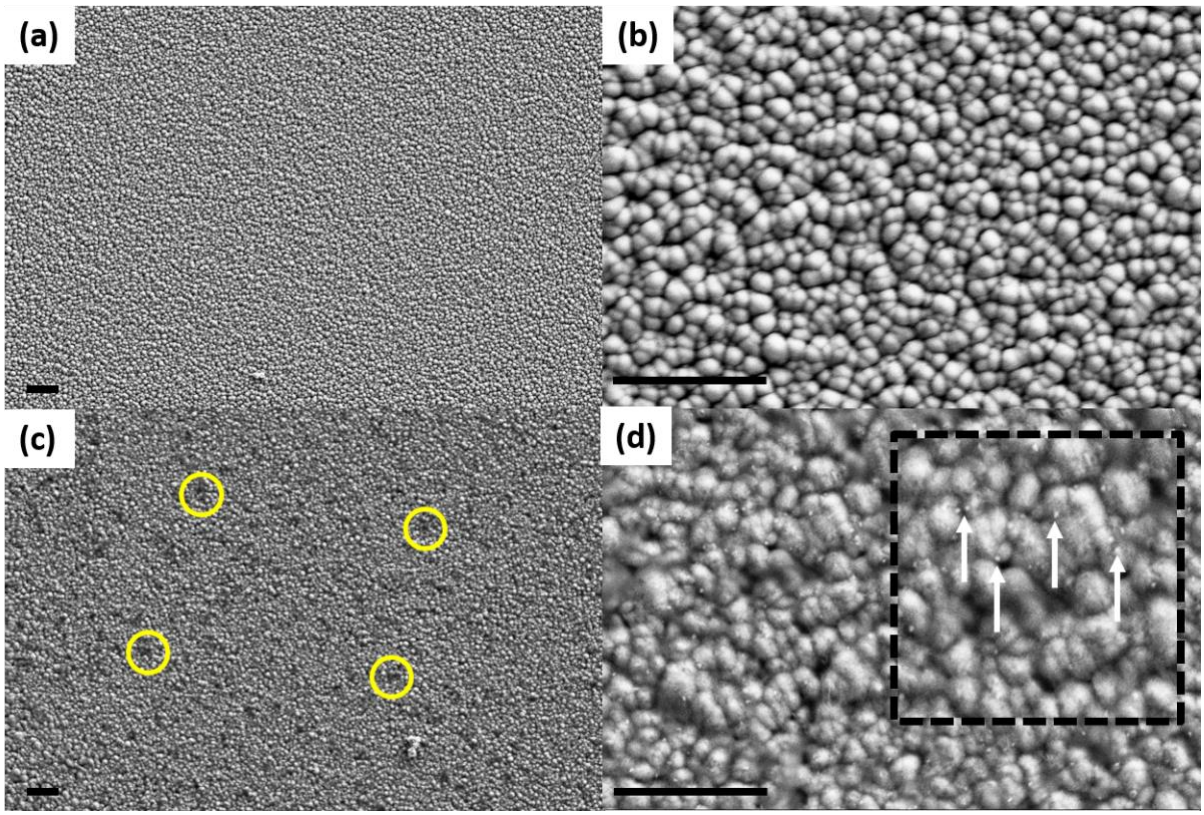

Fig. 6. FESEM images of Cu_2O films (a, b) and Cu_2O films after plasma functionalisation (c,d). circles in (C) and squared [d] shows change in surface morphology with the evolution of nanostructures after exposure to plasma. Scale bar : 2 microns.

Fig. 6 shows the surface morphology for the copper oxide films before and after the plasma treatment. A uniform and compact film can be observed for the Cu_2O sample. The grains are distinctively visible for the Cu_2O sample. The relatively large grain size of the deposited films is due to the 300 W sputtering power. Our previous study shows that the grain size strongly depends on the sputtering power. At this sputtering power (300 W), the films showed the best performance in PEC tests.[16] Mostly due to large grain size leading to increased electrode/electrolyte interfacial contact and decreased grain boundaries reducing the recombination of photogenerated charge carriers. After plasma functionalisation noticeable patterns (highlighted dark spots) are formed on the surface of the film (Fig. 5 (c)). It has been

reported that by introducing nanoscale surface features, catalytic activity can be increased. This is commonly used to increase the surface area of conducting electrodes in electrochemical reactions.[51] In Fig. 5 (d) after plasma functionalisation nanoscale particulate features are obvious. These features could be the early stages of CuO nanowire growth and can be explained based on solid–liquid–solid model (SLS). APPJ consists of several dissociated oxygen species. These highly active oxygen radical diffuse into the surface and due to surface tension and forms a nucleation site for the nanowires.[52] Presence of this features may enhance the electrochemical property of the composite electrode. Interestingly, after plasma functionalisation AFM measurements showed decrease in rms surface roughness from 22.2 nm to 16 nm with plasma treatment. This could be due to the formation of CuO over the Cu_2O base layer. Another possibility could be the ion induced etching of the surface. APPJs has been used for polishing and machining of surfaces at the atomic scale.[53]

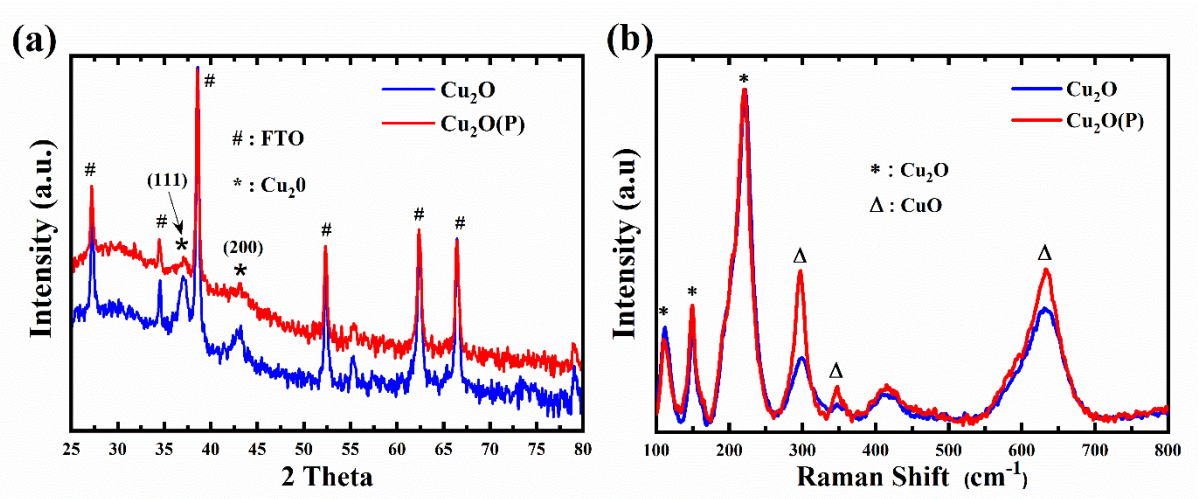

Fig. 7. (a) XRD and (b) Raman spectra of Cu_2O and plasma functionalised Cu_2O thin films.

Figure 7(a) shows the X-ray diffraction pattern of the FTO-supported Cu_2O films before and after plasma functionalisation. Due to the thin nature of films (300nm) the diffraction spectra are dominated by the signal from base FTO. Notably, the peaks corresponding to (111) and (200) planes of cubic Cu_2O are discernible in both the diffraction patterns.[21] However, after plasma treatment the intensity of these peaks decreased, indicating the change in crystal structure of Cu_2O. Raman spectroscopy is a powerful technique to depict the structural properties of metal oxide thin films. The oxides of copper show significantly different Raman signatures, unlike the XRD patterns. As the vibrational properties of this materials are dependent on their crystal symmetry. The influence of plasma functionalisation on the crystal structure of these copper oxide thin films has been further elucidated with micro-Raman spectroscopy as shown in Fig. 7. The presence of Cu_2O as the major phase in both the samples is reflected by the strong peak around 218 cm^{-1}[38]. The intensity of the peak reflects to the highly ordered and crystalline structures of the Cu_2O film. This is one of the Raman forbidden modes for the Cu_2O state, which becomes active due to the breakdown of selection rules. Along with the intense 218 cm^{-1} peak, the peaks around 109, 149, 630 cm^{-1} reflects to the existence of copper in Cu^+ oxidation state in the bulk. [54] This dominant peak at 218 cm^{-1} arises the second-order Raman-allowed $2\,\Gamma_{12}^-$ mode of Cu_2O while the peak around 149 cm^{-1} arises due to the Raman scattering from phonons of F_{1u} symmetry. The broad peak around 417 cm^{-1} arises due to first order scattering of four phonons, three of Γ_{12}^- symmetry and one of Γ_{25}^- symmetry. The peak at 108 cm^{-1} is should have been inactive but has become active due to abundance of defects in the lattice, may be from oxygen vacancies. However, the presence of less intense peaks at 297 cm^{-1}, 347 cm^{-1} signifies to the co-existence of CuO phase in the high temperature annealed thin films. [38] The broad peak around 630 cm^{-1} may not be identified to a particular phase, as both the CuO and Cu_2O has spectral features at this wavenumber. The peak at 297 cm^{-1} with a shoulder peak at 347 cm^{-1} corresponding to the Raman-allowed A_g and B_g^1

mode of CuO respectively becomes noticeably intense after plasma treatment. [15] This signifies that the oxidation and phase change happen not only at the surface partially at the bulk as well. The absence of peak at 529 cm^{-1} shows there is no formation of paramelaconite phase Cu_4O_3. Hence the thin films are a bi phase of CuO and Cu_2O system.

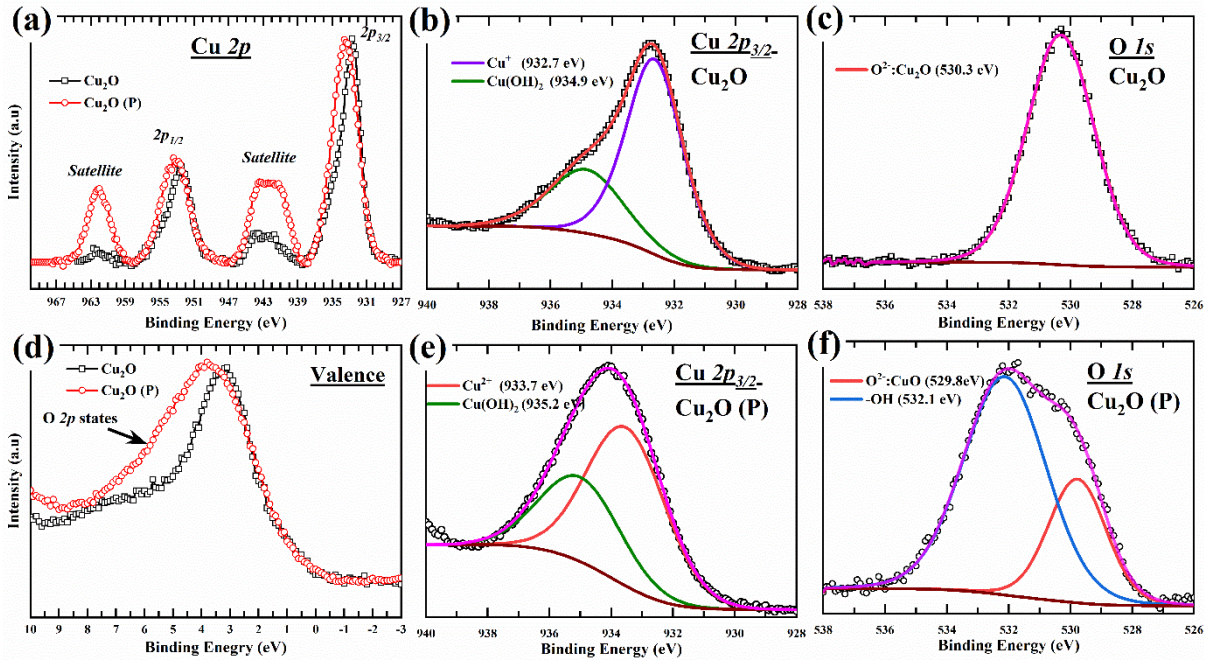

Fig. 8. (a) Difference in Cu 2*p* core level spectra before and after plasma functionalisation (b) fitted Cu $2p_{3/2}$ spectra for Cu_2O (c) fitted O1*s* peak for Cu_2O (d) Valence band features for Cu_2O and Cu_2O/CuO (e) fitted Cu $2p_{3/2}$ spectra for Cu_2O/CuO (f) fitted O1*s* peak for Cu_2O/CuO.

XPS is a highly sensitive technique to determine the surface chemical states of the material under study. Here, XPS has been used to delimit the changes in surface oxidation state after plasma annealing of CuO as all the spectra show significant changes in the line shape. Fig. 8(a) shows the core level Cu2*p* spectra. The binding energies in XPS are strongly dependent on the chemical environment. Hence any change in oxidation state of Cu will reflect as shift or broadening of the line shape at the Cu2*p* core spectra. After plasma functionalisation Cu oxidation state changes from +1($3d^{10}$) to +2($3d^9$). For the pristine sample two main peaks

are observed at 932.7 ± 0.1 and 952.5 ± 0.1 eV corresponding to the $2p_{3/2}$ and $2p_{1/2}$ peaks of Cu_2O respectively. The Cu 2*p* components shifted to higher binding energy values with plasma functionalization. It has been reported that peaks corresponding to the Cu 2*p* states in CuO appear at higher energy positions 933.6 ± 0.3 eV ($2p_{3/2}$) and 953.6 ± 0.4 eV($2p_{1/2}$), along satellite peaks corresponding to electronic shake-up. [55] These are in agreement with our measurements at 933.7 eV and 953.4 eV respectively. Fig. 8 (b) and 8(e) compares the shows the fitted Cu $2p_{3/2}$ spectra for the pristine and plasma functionalised samples. Pristine sample showed contribution from two states at 932.7 eV and 934.9 eV while the other showed peaks at 933.7 eV and 935.2 eV. The components at 932.7 eV and 933.7 eV are the known $2p_{3/2}$ components for Cu_2O and CuO respectively.[18] Ghijsen *et al.* reported that the $2p_{3/2}$ peak for Cu_2O appears at significantly narrower (1.9 eV FWHM) than same peak of CuO (3.4 eV FWHM). For us the FWHM were found to be 2 eV for Cu_2O and 3.1eV for CuO. Both the samples showed a high energy component around 935 ± 0.2 eV due to formation of surface copper hydroxide. Fig. 8 (c) and 8(f) shows the O *1s* core level spectra of the two samples. The line shape for the annealed sample is symmetric and can be fitted with only one peak at 530.3 eV and can be attributed to the lattice oxygen of Cu_2O. However, the other states present the Cu $2p_{3/2}$ spectra are not reflected in here. The line shape of O *1s* spectra changed considerably for the plasma functionalised sample. The peak can be resolved by fitting with two components. The component at 529.8 eV corresponds to the lattice oxygen in CuO. The component at high binding energy 532.1 eV is usually attributed to hydroxyl groups. However, APPJ consists of abundant dissociated oxygen species both ionized and neutral and can considerably influence the surface chemistry of the material. Hence the broad nature of this peak can be from multiple contributions such as chemisorbed dissociated oxygen species (O_2, O^{2-} or O^-) along with OH^-. The high energy shift with respect to reported values for hydroxyl radical (531.5 eV) can be due to the increase polar nature of the bonded hydrogel group. This increase in oxygen density

of states is also reflected in the valence band spectra (Fig. 8 (d)). For copper oxides the O 2*p* derived states contribute to the features between 4 to 8 eV and the Cu 3*d* states are located in the energy range of 4 to 1.5 eV.[55] Valence band for pristine sample shows mainly the Cu 3*d* contributions with less prominent features due to the O 2*p* states this is consistent with the reported Cu_2O spectra. After surface oxidation the O 2*p* intensities dominate at the higher energy, as the 3*d* configuration of Cu^{2+} is lower in energy due to reduce Coulomb repulsion.

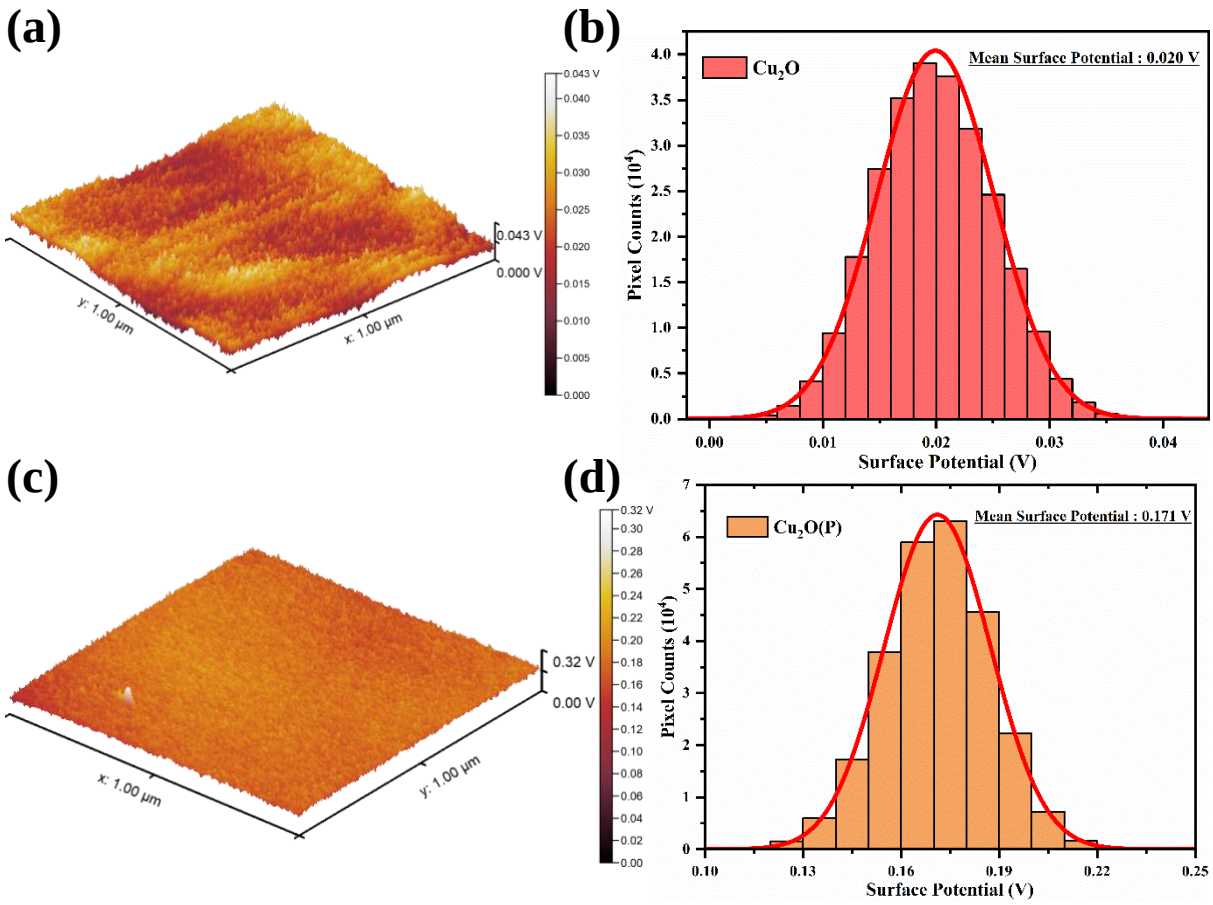

Fig. 9. (a,c) surface potential map for Cu_2O, Cu_2O/CuO (b,d) corresponding surface potential distribution from surface potential map.

To further elucidate the enhancement in catalytic activity after plasma treatment Scanning Kelvin probe microscopy (SKPM) was carried out on these semiconductor surfaces. In SKPM, a conducting tip raster's over the sample surface and detects the surface potential (SP) as the difference in work function between the tip and the sample surface, i.e. SP = $\Phi_{Tip} - \Phi_{Sample}$.[56] It has been reported, that work function of the electrode material play a critical role for electron and proton transfer in the double layer and defines the rate of catalysis.[57] Increasing work function decreases the activation energy and in turn weakens the bond between electrode and chemisorbed oxygen, the cleavage of which is rate limiting for OER activity. In our case we have achieved in reducing the work function and increasing SP via plasma functionalisation by 0.15 V (Fig. 9). It can be due to the formation polar hydroxyl radicals as revealed form XPS. After plasma functionalisation the Fermi level is negatively shifted towards the water redox potential favouring the electron transfer processes require for OER and HER. Also the formation of CuO on top of Cu_2O creates a large space charge region which significantly improves the electron-hole separation efficiency and lowers the electron-hole recombination rate. [21] This ensures a fast charge transport between copper oxides, which enhances the PEC HER activity of the electrodes at cathodic potentials.

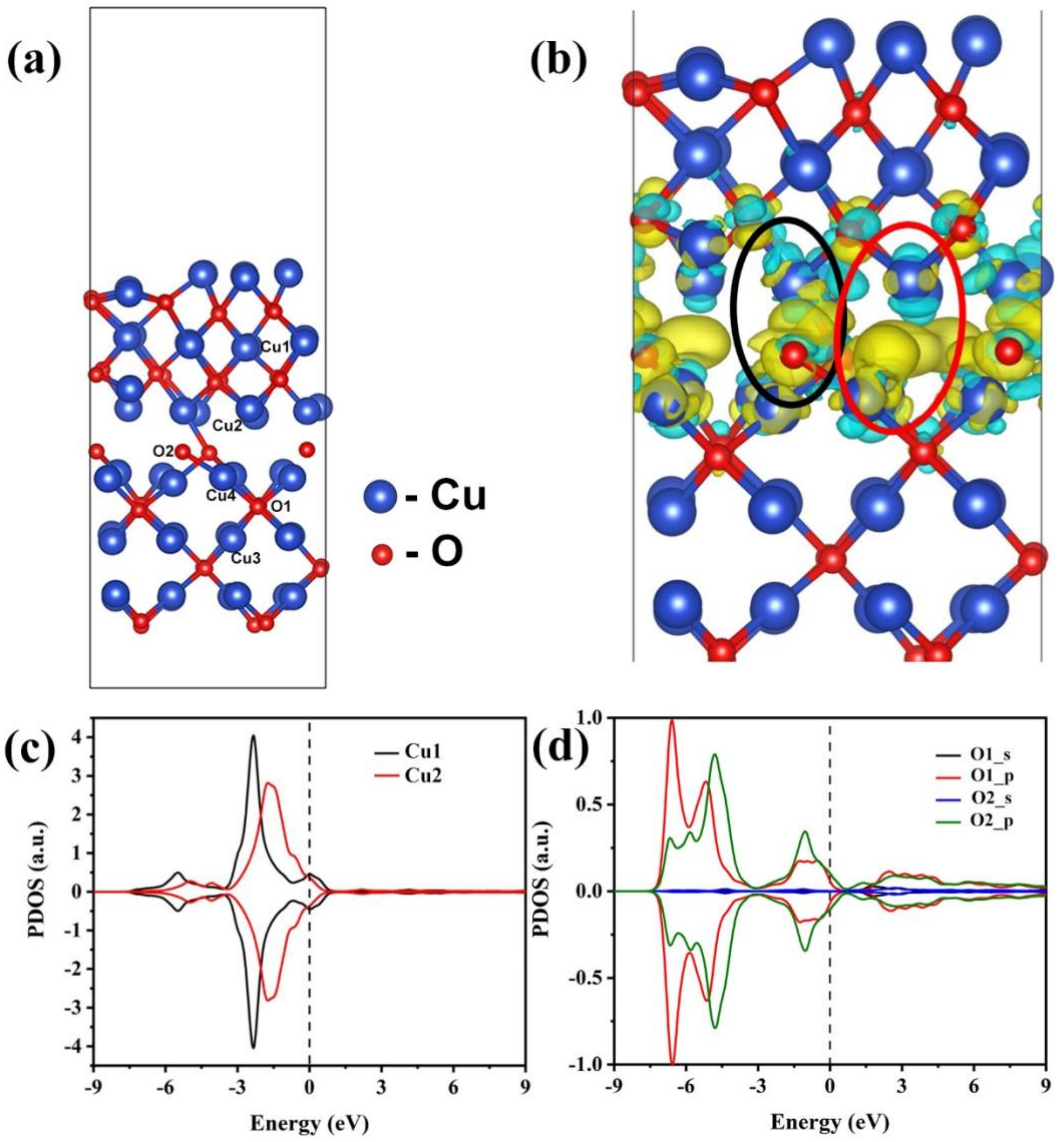

Fig. 10. (a) Model of CuO/Cu_2O heterostructure; Blue and red spheres indicate Cu and O atoms respectively. (b) Charge density difference plot between CuO and Cu_2O layers. Yellow and blue lobes indicate charge accumulation and charge depletion region. The isosurface value taken is 0.003 eV/Å. Inner black and red ellipse refer Cu and O and Cu and Cu interaction. (c) Partial density of states of *d*-orbital of Cu1 and Cu2 atoms. (d) Partial density of states of s and p-orbitals of O1 and O2 atoms.

Having shown the noticeable enhancement in OER and HER activity, in this section, we investigate the role of the heterojunction using density functional theory (DFT) calculations

Initially the model structure was relaxed and the structure after relaxation is shown in Fig. 10 (a). Then density of states is calculated to compare the contribution of Cu and O atoms at the interface and those atoms present deep in the structure. The calculated electronic structures are shown in Fig. 10 (c) & (d). From the electronic structure, Cu2 atom of CuO near the interface has more density of states near fermi level while Cu1 atom from deep in the structure has relatively less states near fermi level (refer to Fig. 10 (a)). As for the oxygen atom, atom from the interface has more density of states near Fermi level. The major contributions are from the *p*-orbital compared to the *s*-orbital, for both the O atom at the interface and that atom present inside. From the charge density difference calculated between the CuO and Cu_2O, two types of transfers are seen. In one case, there is charge accumulation between the O atom from the Cu_2O layer and Cu atom from the CuO layer (indicated inside black ellipse in Fig. 10-b). In another case, there is charge accumulation between the Cu atom from CuO and Cu_2O layers (indicated inside red ellipse in Fig. 10(b)) which indicate possibility in Cu clusters formation in the heterostructure. To support the electronic structure and charge density difference study we have calculated the d-band centre of Cu atoms and *p*-band centre of O atoms (see Table 2). The band centre is given by

$$\frac{\int_{-\infty}^{0} \rho_{d/p} E dE}{\int_{-\infty}^{0} \rho_{d/p} dE} \qquad (1)$$

Here ρ denote the density of *d* and *p*-electron and E denotes the energy eigen value. Cu2 from CuO at the interface has the *d*-band centre near the fermi level, (-1.93 eV) compared to the Cu1 atom from the deep (-2.72 eV). This shift in the *d*-band centre explains more density of states near fermi level of the Cu2 atom at the interface relative to the Cu1 atom from the deep. The charge accumulation between the Cu atom in CuO and O & Cu atoms from the Cu_2O layer. The *p*-band centre of O1 atom belonging to Cu_2O from deep is positioned at -4.97 eV while the *p*-band centre of O2 atom at the interface is at -4.22 eV. This *p*-band centre shift of 0.75

eV of O_2 atom at the interface towards the fermi level makes it more active. The *d*-band centre of the Cu atoms of Cu_2O from deep (Cu3 = -2.25 eV) as well as the interface (Cu4 = -2.23 eV) does not show any significant difference in the shifting towards the fermi level. These results show that the chare transfer happens between the O atom of Cu_2O and Cu atom of CuO at the interface, which contribute to the increased catalytic activity of the heterostructure. Hence, the ability to create an interface with low density of defects is the major advantage of the proposed technique.

Atom	**Band centre (eV)**
Cu1 (deep layer CuO)	-2.72
Cu2 (interface CuO)	-1.93
O1 (deep layer Cu_2O)	-4.97
O2 (interface Cu_2O)	-4.22
Cu3 (deep layer Cu_2O)	-2.25
Cu4 (interface Cu_2O)	-2.23

Table 2. The value of *d* and *p* band centres of Cu and O atoms respectively. The Fermi level is at 0 eV.

4. Conclusion

In summary, the present study shows an important finding through fabrication of CuO/Cu_2O heterojunctions using APPJ functionalisation. With APPJ it is not only possible to tune the surface electronic states but the crystal structure as well. Highly efficient Cu_2O/CuO bilayer composite photocathodes were successfully prepared by a two-step process. First conducting Cu_2O films were obtained by high temperature annealing CuO films followed by oxidation using an APPJ. The oxygen rich environment in the APPJ supressed the creation of copper vacancies which act as recombination centres. The growth of nanostructured CuO form Cu_2O suppressed the lattice defects at the interface. Through theoretical modelling (DFT) we showed that by passivating the defects such as oxygen vacancies and copper defects at the heterojunction we were able to achieve the enhanced catalytic activity. XPS showed the formation of CuO at the surface along the presence of polar hydroxyl radicals enhancing the O2*p* states in the valence region. Raman spectra confirmed that the bulk remained in Cu_2O phase. The composite electrode showed significantly high activity towards OER and photocatalytic HER even without using any conductive substrate as the current collector. For the OER activity the composite electrode showed stability towards OER for up to 2 hours at a current density of 6 $mAcm^{-2}$ in 1M KOH (pH 14) at the same potential the electrodes on FTO substrate could achieve a current ~ 40 $mAcm^{-2}$. When used as a photocathode (non FTO), these electrodes achieved 1.9 $mAcm^{-2}$ at 0 V vs. RHE under AM 1.5 G irradiation. Which is till date the highest photocurrent for a copper oxide electrode without involving any current collector. Additionally, the photocatalytic activity of the films was tested towards photo degradation of Methylene Blue and Phenol. The composite films showed faster degradation of the pollutants compared to the base Cu_2O with a time period of 3 hour. This work presents an attractive route to interface engineering and opens future pathways to directly functionalize copper substrates with APPJ for low cost and high-performance water electrolysers.

Declaration of competing interest

The authors declare no conflict of interest.

Acknowledgements

The work of A.D. and S.K. are funded by UKIERI British Council grant and Royal Academy of Engineering Industry Academia program on Recycling Lithium Ion Batteries and Plasma functionalization of solar cell from Royal Society grant.

References

[1] C. Wadia, A.P. Alivisatos, D.M. Kammen, Materials Availability Expands the Opportunity for Large-Scale Photovoltaics Deployment, Environ. Sci. Technol. 43 (2009) 2072–2077. https://doi.org/10.1021/es8019534.

[2] M.G. Walter, E.L. Warren, J.R. McKone, S.W. Boettcher, Q. Mi, E.A. Santori, N.S. Lewis, Solar water splitting cells, Chem. Rev. 110 (2010) 6446–6473. https://doi.org/10.1021/cr1002326.

[3] X. Liu, S. Cui, Z. Sun, Y. Ren, X. Zhang, P. Du, Self-Supported Copper Oxide Electrocatalyst for Water Oxidation at Low Overpotential and Confirmation of Its Robustness by Cu K-Edge X-ray Absorption Spectroscopy, J. Phys. Chem. C. 120 (2016) 831–840. https://doi.org/10.1021/acs.jpcc.5b09818.

[4] N.T. Suen, S.F. Hung, Q. Quan, N. Zhang, Y.J. Xu, H.M. Chen, Electrocatalysis for the oxygen evolution reaction: Recent development and future perspectives, Chem. Soc. Rev. 46 (2017) 337–365. https://doi.org/10.1039/c6cs00328a.

[5] S.M. Pawar, B.S. Pawar, B. Hou, J. Kim, A.T. Aqueel Ahmed, H.S. Chavan, Y. Jo, S. Cho, A.I. Inamdar, J.L. Gunjakar, H. Kim, S. Cha, H. Im, Self-assembled two-dimensional copper oxide nanosheet bundles as an efficient oxygen evolution reaction (OER) electrocatalyst for water splitting applications, J. Mater. Chem. A. 5 (2017) 12747–12751. https://doi.org/10.1039/c7ta02835k.

[6] G. Li, S. Li, J. Ge, C. Liu, W. Xing, Discontinuously covered IrO2-RuO2@Ru electrocatalysts for the oxygen evolution reaction: How high activity and long-term durability can be simultaneously realized in the synergistic and hybrid nano-structure, J. Mater. Chem. A. 5 (2017) 17221–17229. https://doi.org/10.1039/c7ta05126c.

[7] T. Audichon, T.W. Napporn, C. Canaff, C. Morais, C. Comminges, K.B. Kokoh, IrO2 Coated on RuO2 as Efficient and Stable Electroactive Nanocatalysts for Electrochemical Water Splitting, J. Phys. Chem. C. 120 (2016) 2562–2573. https://doi.org/10.1021/acs.jpcc.5b11868.

[8] M.D. Kärkäs, B. Åkermark, Water oxidation using earth-abundant transition metal catalysts: Opportunities and challenges, Dalt. Trans. 45 (2016) 14421–14461. https://doi.org/10.1039/c6dt00809g.

[9] I. Roger, M.D. Symes, First row transition metal catalysts for solar-driven water oxidation produced by electrodeposition, J. Mater. Chem. A. 4 (2016) 6724–6741. https://doi.org/10.1039/c5ta09423b.

[10] M.B. Gawande, A. Goswami, F.-X.X. Felpin, T. Asefa, X. Huang, R. Silva, X. Zou, R. Zboril, R.S. Varma, Cu and Cu-Based Nanoparticles: Synthesis and Applications in Catalysis., Chem. Rev. 116 (2016) 3722–3811. https://doi.org/10.1021/acs.chemrev.5b00482.
[11] Y. Li, H. Yang, G. Wang, B. Ma, Z. Jin, Distinctive Improved Synthesis and Application Extensions Graphdiyne for Efficient Photocatalytic Hydrogen Evolution, ChemCatChem. 12 (2020) 1985–1995. https://doi.org/10.1002/cctc.201902405.
[12] L. Zhang, G. Wang, X. Hao, Z. Jin, Y. Wang, MOFs-derived Cu3P@CoP p-n heterojunction for enhanced photocatalytic hydrogen evolution, Chem. Eng. J. 395 (2020) 125113. https://doi.org/10.1016/j.cej.2020.125113.
[13] Z. Jin, L. Zhang, G. Wang, Y. Li, Y. Wang, Graphdiyne formed a novel CuI-GD/g-C3N4S-scheme heterojunction composite for efficient photocatalytic hydrogen evolution, Sustain. Energy Fuels. 4 (2020) 5088–5101. https://doi.org/10.1039/d0se01011a.
[14] Z. Jin, L. Zhang, Performance of Ni-Cu bimetallic co-catalyst g-C3N4 nanosheets for improving hydrogen evolution, J. Mater. Sci. Technol. 49 (2020) 144–156. https://doi.org/10.1016/j.jmst.2020.02.025.
[15] S. Masudy-Panah, R. Siavash Moakhar, C.S. Chua, A. Kushwaha, T.I. Wong, G.K. Dalapati, Rapid thermal annealing assisted stability and efficiency enhancement in a sputter deposited CuO photocathode†, RSC Adv. 6 (2016) 29383–29390. https://doi.org/10.1039/c6ra03383k.
[16] S. Masudy-Panah, R. Siavash Moakhar, C.S. Chua, H.R. Tan, T.I. Wong, D. Chi, G.K. Dalapati, Nanocrystal Engineering of Sputter-Grown CuO Photocathode for Visible-Light-Driven Electrochemical Water Splitting, ACS Appl. Mater. Interfaces. 8 (2016) 1206–1213. https://doi.org/10.1021/acsami.5b09613.
[17] H. Xu, J.X. Feng, Y.X. Tong, G.R. Li, Cu2O-Cu Hybrid Foams as High-Performance Electrocatalysts for Oxygen Evolution Reaction in Alkaline Media, ACS Catal. 7 (2017) 986–991. https://doi.org/10.1021/acscatal.6b02911.
[18] J. Han, X. Zong, X. Zhou, C. Li, Cu2O/CuO photocathode with improved stability for photoelectrochemical water reduction, RSC Adv. 5 (2015) 10790–10794. https://doi.org/10.1039/c4ra13896a.
[19] M.B. Gawande, A. Goswami, F.X. Felpin, T. Asefa, X. Huang, R. Silva, X. Zou, R. Zboril, R.S. Varma, Cu and Cu-Based Nanoparticles: Synthesis and Applications in Catalysis, Chem. Rev. 116 (2016) 3722–3811. https://doi.org/10.1021/acs.chemrev.5b00482.
[20] A. Paracchino, V. Laporte, K. Sivula, M. Grätzel, E. Thimsen, Highly active oxide photocathode for photoelectrochemical water reduction, Nat. Mater. 10 (2011) 456–461. https://doi.org/10.1038/nmat3017.
[21] Y. Yang, D. Xu, Q. Wu, P. Diao, Cu2O/CuO bilayered composite as a high-efficiency photocathode for photoelectrochemical hydrogen evolution reaction, Sci. Rep. 6 (2016) 35158. https://doi.org/10.1038/srep35158.
[22] H.-J. Ahn, H.-S. Shim, W.B. Kim, Y.E. Sung, T.-Y. Seong, Co-sputtering growth and electro-oxidation properties of Pt–CuO nanocomposites for direct methanol thin film fuel cells, J. Alloys Compd. 471 (2009) L39–L42. https://doi.org/10.1016/J.JALLCOM.2008.04.008.
[23] S.D. Tilley, M. Schreier, J. Azevedo, M. Stefik, M. Graetzel, Ruthenium Oxide Hydrogen Evolution Catalysis on Composite Cuprous Oxide Water-Splitting Photocathodes, Adv. Funct. Mater. 24 (2014) 303–311. https://doi.org/10.1002/adfm.201301106.
[24] C.G. Morales-Guio, S.D. Tilley, H. Vrubel, M. Grätzel, X. Hu, Hydrogen evolution from

a copper(I) oxide photocathode coated with an amorphous molybdenum sulphide catalyst, Nat. Commun. 5 (2014) 3059. https://doi.org/10.1038/ncomms4059.
[25] S. Masudy-Panah, R. Siavash Moakhar, C.S. Chua, A. Kushwaha, G.K. Dalapati, Stable and Efficient CuO Based Photocathode through Oxygen-Rich Composition and Au-Pd Nanostructure Incorporation for Solar-Hydrogen Production, ACS Appl. Mater. Interfaces. 9 (2017) 27596–27606. https://doi.org/10.1021/acsami.7b02685.
[26] A. Kargar, Y. Jing, S.J. Kim, C.T. Riley, X. Pan, D. Wang, ZnO/CuO heterojunction branched nanowires for photoelectrochemical hydrogen generation, ACS Nano. 7 (2013) 11112–11120. https://doi.org/10.1021/nn404838n.
[27] J. Li, H. Li, Y. Xue, H. Fang, W. Wang, Facile electrodeposition of environment-friendly Cu 2 O/ZnO heterojunction for robust photoelectrochemical biosensing, Sensors Actuators, B Chem. 191 (2014) 619–624. https://doi.org/10.1016/j.snb.2013.10.060.
[28] M.E. Aguirre, R. Zhou, A.J. Eugene, M.I. Guzman, M.A. Grela, Cu2O/TiO2 heterostructures for CO2 reduction through a direct Z-scheme: Protecting Cu2O from photocorrosion, Appl. Catal. B Environ. 217 (2017) 485–493. https://doi.org/10.1016/j.apcatb.2017.05.058.
[29] Q. Shi, G. Ping, X. Wang, H. Xu, J. Li, J. Cui, H. Abroshan, H. Ding, G. Li, CuO/TiO 2 heterojunction composites: An efficient photocatalyst for selective oxidation of methanol to methyl formate, J. Mater. Chem. A. 7 (2019) 2253–2260. https://doi.org/10.1039/c8ta09439j.
[30] A. Paracchino, N. Mathews, T. Hisatomi, M. Stefik, S.D. Tilley, M. Grätzel, Ultrathin films on copper(i) oxide water splitting photocathodes: A study on performance and stability, Energy Environ. Sci. 5 (2012) 8673–8681. https://doi.org/10.1039/c2ee22063f.
[31] A.A. Dubale, W.N. Su, A.G. Tamirat, C.J. Pan, B.A. Aragaw, H.M. Chen, C.H. Chen, B.J. Hwang, The synergetic effect of graphene on Cu2O nanowire arrays as a highly efficient hydrogen evolution photocathode in water splitting, J. Mater. Chem. A. 2 (2014) 18383–18397. https://doi.org/10.1039/c4ta03464c.
[32] Z. Zhang, R. Dua, L. Zhang, H. Zhu, H. Zhang, P. Wang, Carbon-layer-protected cuprous oxide nanowire arrays for efficient water reduction, ACS Nano. 7 (2013) 1709–1717. https://doi.org/10.1021/nn3057092.
[33] H. Wu, Z. Zheng, C.Y. Toe, X. Wen, J.N. Hart, R. Amal, Y.H. Ng, A pulse electrodeposited amorphous tunnel layer stabilises Cu2O for efficient photoelectrochemical water splitting under visible-light irradiation, J. Mater. Chem. A. 8 (2020) 5638–5646. https://doi.org/10.1039/d0ta00629g.
[34] A.A. Dubale, A.G. Tamirat, H.M. Chen, T.A. Berhe, C.J. Pan, W.N. Su, B.J. Hwang, A highly stable CuS and CuS-Pt modified Cu2O/CuO heterostructure as an efficient photocathode for the hydrogen evolution reaction, J. Mater. Chem. A. 4 (2016) 2205–2216. https://doi.org/10.1039/c5ta09464j.
[35] Y.F. Lim, C.S. Chua, C.J.J. Lee, D. Chi, Sol-gel deposited Cu2O and CuO thin films for photocatalytic water splitting, Phys. Chem. Chem. Phys. 16 (2014) 25928–25934. https://doi.org/10.1039/c4cp03241a.
[36] Z. Zhang, P. Wang, Highly stable copper oxide composite as an effective photocathode for water splitting via a facile electrochemical synthesis strategy, J. Mater. Chem. 22 (2012) 2456–2464. https://doi.org/10.1039/c1jm14478b.
[37] A.A. Dubale, C.J. Pan, A.G. Tamirat, H.M. Chen, W.N. Su, C.H. Chen, J. Rick, D.W. Ayele, B.A. Aragaw, J.F. Lee, Y.W. Yang, B.J. Hwang, Heterostructured Cu2O/CuO decorated with nickel as a highly efficient photocathode for photoelectrochemical water reduction, J. Mater. Chem. A. 3 (2015) 12482–12499.

https://doi.org/10.1039/c5ta01961c.
[38] Y. Deng, A.D. Handoko, Y. Du, S. Xi, B.S. Yeo, In Situ Raman Spectroscopy of Copper and Copper Oxide Surfaces during Electrochemical Oxygen Evolution Reaction: Identification of CuIII Oxides as Catalytically Active Species, ACS Catal. 6 (2016) 2473–2481. https://doi.org/10.1021/acscatal.6b00205.
[39] S.K. Baek, J.S. Kim, Y.D. Yun, Y.B. Kim, H.K. Cho, Cuprous/Cupric Heterojunction Photocathodes with Optimal Phase Transition Interface via Preferred Orientation and Precise Oxidation, ACS Sustain. Chem. Eng. 6 (2018) 10364–10373. https://doi.org/10.1021/acssuschemeng.8b01715.
[40] S.M. Pawar, J. Kim, A.I. Inamdar, H. Woo, Y. Jo, B.S. Pawar, S. Cho, H. Kim, H. Im, Multi-functional reactively-sputtered copper oxide electrodes for supercapacitor and electro-catalyst in direct methanol fuel cell applications, Sci. Rep. 6 (2016) 1–9. https://doi.org/10.1038/srep21310.
[41] E. Comini, G. Sberveglieri, C. Sada, D. Barreca, A. Gasparotto, C. Maccato, E. Tondello, Chemical vapor deposition of Cu2O and CuO nanosystems for innovative gas sensors, in: Proc. IEEE Sensors, 2009: pp. 111–113. https://doi.org/10.1109/ICSENS.2009.5398223.
[42] A. Dey, A. Lopez, G. Filipič, A. Jayan, D. Nordlund, J. Koehne, S. Krishnamurthy, R.P. Gandhiraman, M. Meyyappan, Plasma jet based in situ reduction of copper oxide in direct write printing, J. Vac. Sci. Technol. B. 37 (2019) 031203. https://doi.org/10.1116/1.5087255.
[43] J. Golda, J. Held, B. Redeker, M. Konkowski, P. Beijer, A. Sobota, G. Kroesen, N.S.J. Braithwaite, S. Reuter, M.M. Turner, T. Gans, D. O'Connell, V. Schulz-Von Der Gathen, Concepts and characteristics of the "COST Reference Microplasma Jet," J. Phys. D. Appl. Phys. 49 (2016) 084003. https://doi.org/10.1088/0022-3727/49/8/084003.
[44] G. Kresse, J. Furthmüller, Efficiency of ab-initio total energy calculations for metals and semiconductors using a plane-wave basis set, Comput. Mater. Sci. 6 (1996) 15–50.
[45] P.E. Blöchl, Projector augmented-wave method, Phys. Rev. B. 50 (1994) 17953–17979. https://doi.org/10.1103/PhysRevB.50.17953.
[46] J.P. Perdew, K. Burke, M. Ernzerhof, Generalized gradient approximation made simple, Phys. Rev. Lett. 77 (1996) 3865–3868. https://doi.org/10.1103/PhysRevLett.77.3865.
[47] C.W. Li, M.W. Kanan, CO 2 reduction at low overpotential on Cu electrodes resulting from the reduction of thick Cu 2O films, J. Am. Chem. Soc. 134 (2012) 7231–7234. https://doi.org/10.1021/ja3010978.
[48] S. Sai Guru Srinivasan, B. Govardhanan, P. Aabel, M. Ashok, M.C. Santhosh Kumar, Effect of oxygen partial pressure on the tuning of copper oxide thin films by reactive sputtering for solar light driven photocatalysis, Sol. Energy. 187 (2019) 368–378. https://doi.org/10.1016/j.solener.2019.05.057.
[49] C. Feng, Z. Chen, J. Jing, J. Hou, The photocatalytic phenol degradation mechanism of Ag-modified ZnO nanorods, J. Mater. Chem. C. 8 (2020) 3000–3009. https://doi.org/10.1039/c9tc05010h.
[50] M. Hayyan, M.A. Hashim, I.M. Alnashef, Superoxide Ion: Generation and Chemical Implications, Chem. Rev. 116 (2016) 3029–3085. https://doi.org/10.1021/acs.chemrev.5b00407.
[51] J. Li, X. Jin, R. Li, Y. Zhao, X. Wang, X. Liu, H. Jiao, Copper oxide nanowires for efficient photoelectrochemical water splitting, Appl. Catal. B Environ. 240 (2019) 1–8. https://doi.org/10.1016/j.apcatb.2018.08.070.
[52] G. Filipič, U. Cvelbar, Copper oxide nanowires: a review of growth, Nanotechnology. 23 (2012) 194001. https://doi.org/10.1088/0957-4484/23/19/194001.

[53] J. Zhang, B. Wang, S. Dong, Application of atmospheric pressure plasma polishing method in machining of silicon ultra-smooth surfaces, Front. Electr. Electron. Eng. China. 3 (2008) 480–487. https://doi.org/10.1007/s11460-008-0072-9.
[54] T. Sander, C.T. Reindl, M. Giar, B. Eifert, M. Heinemann, C. Heiliger, P.J. Klar, Correlation of intrinsic point defects and the Raman modes of cuprous oxide, Phys. Rev. B. 90 (2014) 045203. https://doi.org/10.1103/PhysRevB.90.045203.
[55] Y. Wang, S. Lany, J. Ghanbaja, Y. Fagot-Revurat, Y.P. Chen, F. Soldera, D. Horwat, F. Mücklich, J.F. Pierson, Electronic structures of C u2 O, C u4 O3, and CuO: A joint experimental and theoretical study, Phys. Rev. B. 94 (2016) 1–10. https://doi.org/10.1103/PhysRevB.94.245418.
[56] A. Dey, P. Ghosh, J. Bowen, N.S.J. Braithwaite, S. Krishnamurthy, Engineering work function of graphene oxide from p to n type using a low power atmospheric pressure plasma jet, Phys. Chem. Chem. Phys. 22 (2020) 7685–7698. https://doi.org/10.1039/c9cp06174f.
[57] C.G. Vayenas, S. Bebelis, S. Ladas, Dependence of catalytic rates on catalyst work function, Nature. 343 (1990) 625–627. https://doi.org/10.1038/343625a0.